Materials Research Express

PAPER

First-principles study of Zn-doping effects on phase stability and magnetic anisotropy of Ni-Mn-Ga alloys

Jozef Janovec[1], **Ladislav Straka**[2,3], **Alexei Sozinov**[4], **Oleg Heczko**[2,3] **and Martin Zelený**[1,2]

[1] Faculty of Mechanical Engineering, Institute of Materials Science and Engineering, Brno University of Technology, Technická 2896/2, CZ-61669 Brno, Czech Republic
[2] Charles University, Faculty of Mathematics and Physics, Institute of Physics, Ke Karlovu 5, CZ-12116 Prague 2, Czech Republic
[3] Institute of Physics of the Czech Academy of Sciences, Na Slovance 1999/2, CZ-18221 Prague, Czech Republic
[4] Material Physics Laboratory, LUT University, Yliopistonkatu 34, 53850 Lappeenranta, Finland

E-mail: jozef.janovec@vutbr.cz

OPEN ACCESS

RECEIVED
4 November 2019

REVISED
19 December 2019

ACCEPTED FOR PUBLICATION
8 January 2020

PUBLISHED
4 February 2020

Keywords: magnetic shape memory alloy, *ab initio* calculations, doping, phase stability, martensitic transformation, Curie temperature, magnetic anisotropy

Supplementary material for this article is available online

Abstract

The effect of Zn doping on Ni-Mn-Ga magnetic shape memory alloy was studied by the first-principles calculations using exact muffin-tin orbital method in combination with the coherent-potential approximation and projector augmented-wave method. Trends in martensitic transformation temperature T_M and Curie temperature T_C were predicted from calculated energy differences between austenite and nonmodulated martensite, $\Delta E_{\mathrm{A-NM}}$, and energy differences between paramagnetic and ferromagnetic state, $\Delta E_{\mathrm{PM-FM}}$. Doping upon the Ga-sublattice results in stabilization of martensitic phase which indicates the increase in T_M. T_C is affected only weakly or slightly decreases, because $\Delta E_{\mathrm{PM-FM}}$ of martensite does not change significantly with doping. The substitution of Mn atoms by Zn causes the decrease in both T_M and T_C. Comparing to Cu-doped Ni-Mn-Ga alloys, we predict that doping with Zn results in smaller decrease in T_C but also in smaller increase in T_M. Moreover, Cu doping upon the Ga-sublattice strongly decreases the magnetic anisotropy energy of martensite, whereas such strong effect was not observed for Zn doping. Based on the calculations of Zn-doped Ni-Mn-Ga alloys we suggest that simultaneous doping with Zn and an element increasing T_C can result in significant increase in both transformation temperatures without strong decrease of magnetic anisotropy.

1. Introduction

Numerous scientific investigations have been done in order to study Ni-Mn-Ga Heusler alloys mainly because they exhibit magnetic shape memory (MSM) behavior. The macroscopic deformation of such materials in an external magnetic field, so called Magnetic Field-Induced Strain (MFIS), is caused by the motion of highly mobile twin boundaries in magnetically ordered martensite [1, 2]. Ni-Mn-Ga alloy is known for its 6 % MFIS in martensite with five-layered modulation (10M) [3, 4]. Other martensitic phases observed experimentally in Ni-Mn-Ga systems are seven-layered martensite (14M) with MFIS up to 10 % [5] and nonmodulated martensite (NM), stable far from stoichiometric composition with no MFIS reported [6, 7]. Recently the stability of four-layered modulated martensite (4O) was predicted theoretically [8].

Practical usability of Ni-Mn-Ga is restricted by its low transformation temperature from cubic austenite with $L2_1$ structure to martensite which occurs at $T_M = 202$ K in stoichiometric Ni_2MnGa alloy [9]. The Curie temperature is also relatively low, with $T_C = 376$K. For practical applications in small actuators [10] or energy harvesters [11], all relevant transformations should be at least several tens of kelvins above the room temperature. For more demanding applications e.g. for use in internal combustion engines, all transformation temperatures should be above 413K [12].

There are three ways to increase transformation temperatures: i) by finding an alternative alloy, ii) by changing the stoichiometry of known MSM alloy such as Ni-Mn-Ga, and iii) by doping or alloying the known alloy by additional elements. Simultaneously with improving T_M and T_C one may consider improvement of other application relevant properties such as saturation magnetization, magnetic anisotropy, or mobility of twin boundaries.

It has already been demonstrated experimentally that significant improvements can be achieved by doping and alloying [13, 14]. For example, the alloy $Ni_{46}Co_4Mn_{24}Ga_{22}Cu_4$ shows 12 % MFIS in NM martensite and an increase in both T_M and T_C to 330 K and 393 K, respectively [15]. The increase in T_M in this alloy is caused by the replacement of Cu upon the Ga sublattice, as this element independently can increase T_M by 150 K if 3 at. % of Cu is substituted [16–18]. Increasing concentration of Cu on Ga sublattice is accompanied with a decrease in T_C [17], which has to be compensated by substitution of Ni by Co as an element increasing T_C [19]. However, magnetic anisotropy strongly decreases with increasing concentration of doping elements [20]. Promising results were also documented for alloys doped by Zn, since $Ni_{50}Mn_{25}Ga_{22}Zn_3$ alloy exhibited T_M increased by 114 K [21]. However, fabrication and consequently an experimental study of Ni-Mn-Ga-Zn systems with higher content of Zn are strongly limited due to intensive evaporation of Zn during alloying. Nevertheless, we believe that suitable experimental method, like sputtering or powder metallurgy will be found if Zn is beneficial for Ni-Mn-Ga system. Considering the difficulties in alloy preparation, employing of a computational approach is usefull to predict the properties relevant for MSM behavior such as martensitic transformation temperature T_M, Curie temperature T_C and magnetic anisotropy energy.

One of methods used for theoretical prediction of T_M relates the transformation temperatures with the number of valence electrons per atom e/a [22, 23] and concludes that higher e/a indicates higher T_M. If we consider Mn having 7 valence electrons in d and s orbitals and Ga having 3 valence electrons in p and s orbitals, $T_M \sim e/a$ rule is very well applicable for off-stoichiometric alloys [23]. The same rule was applied also for alloys containing Cu. Considering its 11 valence electrons, the addition of Cu instead of Ga significantly increases the e/a ratio, which corresponds to a significant increase in T_M [16, 17, 24, 25]. Here we expand this approach further by selecting Zn-doping. One can expect that Zn, having 12 valence electrons, increases T_M even more than Cu. Simultaneously, atomic radius of Zn is about the same as atomic radius of Ga atom (134 pm vs 135 pm) [26], hence in comparison with influence of Cu-doping (atomic radius of Cu is 128 pm) [26], we can expect small changes in Curie temperature due to lattice contraction [17, 27].

Qualitative predictions of T_M in the present study are based upon its correlation with energy difference between austenite and nonmodulated martensite, ΔE_{A-NM}, taken from the energy profile along the tetragonal deformation path. The increase or decrease in T_M is predicted by comparison of ΔE_{A-NM} in a studied system with ΔE_{A-NM} in a reference system of stoichiometric Ni_2MnGa alloy. If ΔE_{A-NM} for the modified alloy is greater than that for the referential one, an increase in T_M is expected. Similarly, lowering of ΔE_{A-NM} corresponds to the decrease in T_M as was shown for offstoichiometric Ni_2MnGa [28] and Ga_2MnNi alloys [29].

All such predictions are based on an assumption that the entropy contributions to the Gibbs free energy lowers the free energy more or less equally in the systems with the same crystal structure for small concentrations of doping elements. Free energy profiles of corresponding phases in doped and non-doped systems are assumed to have very similar shape but are shifted with respect to each other, as is schematically shown in figure 1. With such assumption, a shift of intersection of austenite and martensite free energy profiles towards higher or lower temperature is directly dependent on the increase or decrease of ΔE_{A-NM} at 0 K. This method, however, provides only qualitative predictions of changes in T_M. For quantitative predictions, it is necessary to know the exact evolution of free energy.

The prediction of Curie temperature T_C works similarly as described for T_M, but here one has to consider not only the contribution of vibrational entropy but particularly the effect of magnetic entropy. In this case T_C should correlate with the energy difference between paramagnetic (PM) and ferromagnetic (FM) state, ΔE_{PM-FM} [30–32]. The validity of these approaches, $T_M \sim \Delta E_{A-NM}$ and $T_C \sim \Delta E_{PM-FM}$, has been established for Co and Cu-doping [24, 33, 34]. Both transformation temperatures can be theoretically predicted by more precise methods including phonon [35] or Monte Carlo [36] calculation, however, with much higher computational cost especially in the case of doped alloys. The less precise but computationaly less expensive approach presented in this paper can be used for fast preselection of alloy composition for further deeper investigation by more precise methods or for experimental preparation.

The purpose of this paper is to find how Zn-doping on both Ga or Mn sublattices affects the stability of austenite with respect to NM martensite. We present a detailed and comprehensive first-principles investigation of total-energy behavior along the tetragonal deformation path for PM and FM states for different compositions which allows us to predict trends in martensitic transformation temperatures T_M and Curie temperature T_C. Moreover, we also determine the heat of formation for studied systems, site preferences of doping atoms, and magnetic anisotropy of martensitic phase. The stability of cubic austenite and tetragonal martensite is evaluated using the density of states (DOS) analysis.

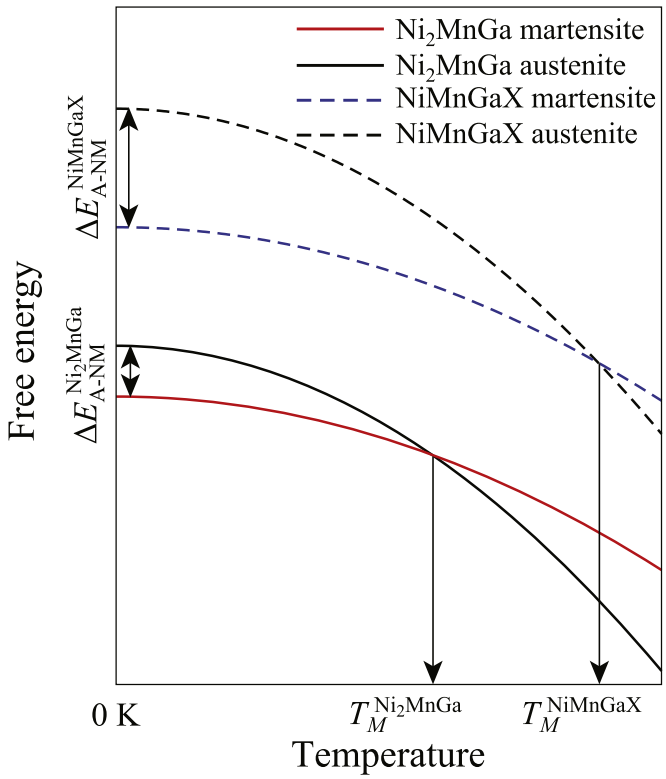

Figure 1. Schematic development of Gibbs free energy as a function of temperature for stoichiometric alloy Ni_2MnGa and an alloy modified by doping Ni-Mn-Ga-X in austenite and martensite. At 0 K, the difference in total energies ΔE_{A-NM} is equal to the difference in free energies. If we suppose both doped and stoichiometric alloys having similar free energy profiles, a change in T_M can be estimated from the comparison of ΔE_{A-NM} in these systems.

2. Computational details

The *ab initio* calculations were performed using the exact muffin-tin orbital (EMTO) method [37, 38] based on an improved Korringa-Kohn-Rostoker (KKR) approach [39]. In combination with the full charge density (FCD) technique [40], the EMTO is suitable to accurately describe the total energy with respect to anisotropic lattice distortions such as tetragonal deformation. The exchange-correlation term was described within the Perdew–Burke–Ernzerhof (PBE) parametrization of generalized gradient approximation [41]. In the self-consistent calculations, the one-electron equations were treated within the scalar-relativistic and soft-core approximations. The EMTO Green's function was calculated for 32 complex energy points distributed exponentially on a semi-circular contour. In the EMTO basis set s, p, d and f orbitals were included and Ni $3d^8\,4s^2$, Mn $3d^5\,4s^2$, Ga $3d^{10}\,4s^2\,4p^1$ and Zn $3d^{10}\,4s^2$ were considered as the valence orbitals. In order to get a better agreement with experiment for non-modulated martensitic structure, the muffin-tin potential on the Ni sublattice was optimized by choosing the atomic radius $R_{ws}^{Ni} = 1.10R_{ws}$ [42] and the overlapping potential sphere radius $R_{mt}^{Ni} = 0.95R_{ws}$, [43] where R_{ws} is the average Wigner-Seitz radius. In the one-center expansion of the full charge density, the number of components was truncated to eight. The Brillouin zone was defined on a $13 \times 13 \times 13$ uniform k-point mesh without any smearing technique. The spin disordered magnetic structure of PM state was simulated using the disordered local moment (DLM) formalism, where the magnetic disorder was represented by randomly distributed Mn atoms with oppositely oriented magnetic moments [44]. Both chemical disorder caused by doping as well as magnetic disorder of PM state were included by using coherent potential approximation (CPA) [45, 46]. The effect of the charge misfit on the spherical potential is taken into account using the screened impurity model in [47] and [48].

Considering previous theoretical and experimental studies, we have chosen doping with 2.5 at. % and 5 at. % of Zn on either the Mn or Ga sublattice. A series of total energies was calculated for each composition at constant volume of austenite in the range between $c/a = 0.9$ and 1.4, which describes the tetragonal deformation of cubic $L2_1$ structure ($c/a = 1$, see Supplementary material available online at stacks.iop.org/MRX/7/026101/mmedia for strucuture of austenite and tetragonaly distorted structure of NM marteniste). All calculated total energies along the deformation path were related to the energy of cubic structure in FM state for alloy with given composition.

Table 1. Comparison of values of standard heat of formation H_f in FM state, total magnetic moment μ_{tot}^{A}, equilibrium volume of austenite in FM and PM states V_{0A}, and equilibrium $(c/a)_{NM}$ of NM martensite in FM state calculated using EMTO-CPA method. Boldface indicates the most stable configurations for each alloy composition.

Alloy	H_f(eV/atom)	μ_{tot}^{A} (μ_B/f.u.)	FM V_{0A} (Å^3)	PM V_{0A} (Å^3)	FM $(c/a)_{NM}$
$Ni_{50}Mn_{25}Ga_{25}$	**−0.305**	**4.11**	**49.11**	**49.18**	**1.252**
$Ni_{50}Mn_{25}(Ga_{20}Zn_5)$	**−0.286**	**4.11**	**48.97**	**49.07**	**1.243**
$Ni_{50}(Mn_{20}Zn_5)(Ga_{20}Mn_5)$	−0.266	2.46	49.00	—	—
$(Ni_{45}Zn_5)Mn_{25}(Ga_{20}Ni_5)$	−0.238	4.09	49.14	—	—
$Ni_{50}(Mn_{20}Zn_5)Ga_{25}$	**−0.312**	**3.28**	**49.10**	**49.17**	**1.202**
$Ni_{50}(Mn_{20}Ga_5)(Ga_{20}Zn_5)$	−0.274	3.32	49.23	—	—
$(Ni_{45}Zn_5)(Mn_{20}Ni_5)Ga_{25}$	−0.268	3.30	49.29	—	—

Magnetic anisotropy energy of NM martensite was computed with the help of force theorem from the energy difference between magnetization along [001] and [100] direction with spin–orbit coupling included in the Kohn–Sham equation while using the same self-consistent scalar-relativistic potential [49]. Thus, the negative MAE corresponds to preferred magnetization in easy plane given by equivalent directions [100] and [010], whereas positive MAE indicates preferred magnetization along easy axis parallel to [001] direction of tetragonal lattice. We used the Vienna Ab initio Simulation Package (VASP) [50, 51] in which the electron-ion interaction was described by projector augmented-wave (PAW) potentials [52, 53]. The electronic orbitals were expanded in terms of plane waves with a maximum kinetic energy of 600 eV. The doping by 6.25 at. % of Zn or Cu on either the Mn or Ga sublattice was modeled by replacement of single atom in 16 atom cell of tetragonally distorted $L2_1$ lattice (see Supplementary matrial). The Brillouin zone (BZ) was sampled using a $12 \times 12 \times 10$ Γ-point-centered mesh. The integration over the BZ used the Methfessel–Paxton smearing method [54] with a 0.02 eV smearing width. The total energy was calculated with high precision by convergence to 10^{-7} eV per computational cell. The structural relaxation was stopped when all forces acting on the atoms converged to within 10^{-3} eV/Å and all relevant components of the stress tensor converged to within 0.1 GPa.

3. Results

3.1. Site preference and equilibrium volume of austenite

The first step in the theoretical investigation of alloys is to find their thermodynamic stability represented by the enthalpy of formation at equilibrium volume and the site preference of doping atoms. The standard enthalpy of formation was obtained from theoretical formula

$$H_f = E_{tot} - \frac{50E_{Ni} + (25 - y)E_{Mn} + (25 - z)E_{Ga} + (y + z)E_X}{100}, \quad (1)$$

which is applicable for the $Ni_{50}Mn_{25-y}Ga_{25-z}X_{y+z}$ system. Here E_{tot} is the total energy of an alloy per atom in FM state and following energies represent total energies of corresponding elements in their standard forms per atom taken as follows: fcc nickel (ferromagnetic), manganese (antiferromagnetic), gallium and hcp zinc. The heat of formation of stoichiometric Ni_2MnGa (or $Ni_{50}Mn_{25}Ga_{25}$) calculated in this work by EMTO-CPA is −0.3052 eV/atom, which agrees with other theoretical (−0.2993 eV/atom calculated by the projector augmented wave method [55]) and experimental results (−0.3089 eV/atom [56]). The site preference of substitutional atoms was determined by the lowest energy of formation. Normal site occupation was compared to anti-site occupancy, when dopant elements occupy other than deficient sublattice. The calculations were performed only for alloys with 5 at. % of doping element. Zinc shows tendency to always occupy sublattices of atoms in deficiency, which is in agreement with previous calculations for Zn-doping at the expense of Ga [57]. The results are summarized in table 1.

Calculations of standard enthalpy of formations as well as the following calculations of tetragonal deformation paths were performed at the equilibrium volume V_{0A} of the austenite $L2_1$ cell over the entire c/a range. The difference between the austenite and NM martensite equilibrium volumes is minimal, especially for low concentrations of dopants and therefore the energies along the deformation path are sufficiently accurate when using the austenite equilibrium volume for every c/a [33]. The results of calculations in FM state show that Zn substitution of Ga decreases V_{0A} and the Zn substitution of Mn does not have significant effect on V_{0A}. Equilibrium volumes in PM states are slightly larger than in FM states with the same effect of doping for all studied compositions. Results for all FM systems as well as for the most stable PM systems are summarized in table 1. The dependency of the equilibrium volume V_{0A} on the concentration of dopant is linear in all considered substitutions and can be described approximately as

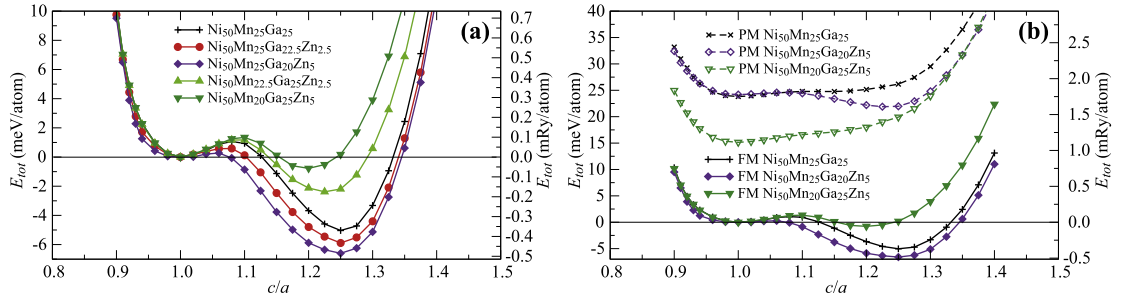

Figure 2. Total energy as a function of c/a along the tetragonal deformation path in FM state for alloys with different Zn concentration (a) and in FM and PM states for alloys with 5 at. % of Zn (b).

$$V_{0A} = V^{*}_{0A} - 0.027\,3z - 0.000\,9y, \tag{2}$$

where V^{*}_{0A} represents the equilibrium volume of stoichiometric alloy and the parameters are the concentration of dopants (z represents concentration of Zn at Ga sites (Zn → Ga) and y represents concentration of Zn at Mn sites (Zn → Mn).

The total magnetic moment per unit cell of austenite, μ^{A}_{tot}, is also listed in table 1. Calculations did not reveal any unusual magnetic behavior of doped alloys. Substitution of Mn atoms resulted in a decrease of total magnetic moment since Mn atoms bear the largest magnetic moment in the alloy. Noticeable decrease of μ^{A}_{tot} in $Ni_{50}(Mn_{20}Zn_5)(Ga_{20}Mn_5)$ is caused by the antiparallel alignment of magnetic moments of Mn atoms on Ga sublattice to the atoms on Mn sublattice [58].

3.2. Tetragonal deformation in FM state

Results obtained for stoichiometric Ni_2MnGa in both FM and PM states, are taken as reference values for all modified alloys. The tetragonal deformation path in FM state shows two energy minima and a barrier between them (figure 2(a)). The minimum occurring at $c/a = 1$ represents the $L2_1$ cubic austenite, the second minimum occurs at $c/a \approx 1.25$ and represents the NM tetragonal martensite. Experimentally observed tetragonality of NM martensite $(c/a)_{NM} \approx 1.17$–1.23 [23] is smaller than calculated value, however, all *ab initio* methods in general overestimate tetragonality [35, 59–62].

The development of energy profiles in figure 2(a) shows clearly that substitution of Mn by Zn leads to both destabilization of NM martensite as well as reduction of its tetragonality $(c/a)_{NM}$. Also, the energy barrier grows and moves towards higher c/a, which indicates additional stabilization of austenite phase. Notably Zn substitution instead of Ga has an opposite effect, as also shown in recent *ab initio* calculations of Zn doping on Ga sublattice with 6.25 and 12.5 at. % [57]. The total energy of NM martensite is lower for modified alloys and the energy barrier between austenite and martensite gets smaller. Both these factors are in favor of more stable NM martensite. The tetragonality changes only slightly.

3.3. Tetragonal deformation in PM state

In order to predict behavior of the Curie temperature, calculations of tetragonal deformation paths were performed in paramagnetic states employing the DLM approximation. Computed tetragonal deformation paths in both FM and PM states for alloys with 5 at. % of Zn are shown in figure 2(b), both magnetic states are related to the energy of the FM austenite of a given composition. The energy profile of Ni_2MnGa in PM state exhibits a global minimum at $c/a = 1$, whereas NM martensite is represented by a very shallow minimum with higher energy at $(c/a)_{NM} = 1.14$ in this magnetic state [34]. Doping on Mn sublattice has an even stronger suppressing effect on PM martensite and simultaneously lowers the austenite energy minimum, which predicts lower stability of FM states. On the contrary, doping on Ga sublattice strongly deepens the NM martensite minimum, which corresponds to similar stabilization effect of Zn on NM martensite found in the FM state.

3.4. Electronic structure

The effect of doping on electronic structure of Ni-Mn-Ga alloys was studied in order to explain observed behavior of total energy profiles and to examine the local stability of austenite. Majority density of states (DOS) channels do not play important role in the stability of Ni-Mn-Ga alloys due to their featureless character around the Fermi level. By analysis of minority spin channel of density of states, we can ascribe the stability of austenite in stoichiometric Ni_2MnGa to formation of a pseudogap about 0.65 eV below the Fermi level, E_f, and a Ni-Ni antibonding peak 0.2 eV below E_f. A shallow and narrow pseudogap indicates weak covalent bonding [63]. Due to the Jahn-Teller effect a distortion of cubic lattice breaks the degeneracy of d bands near E_f and thus causes a

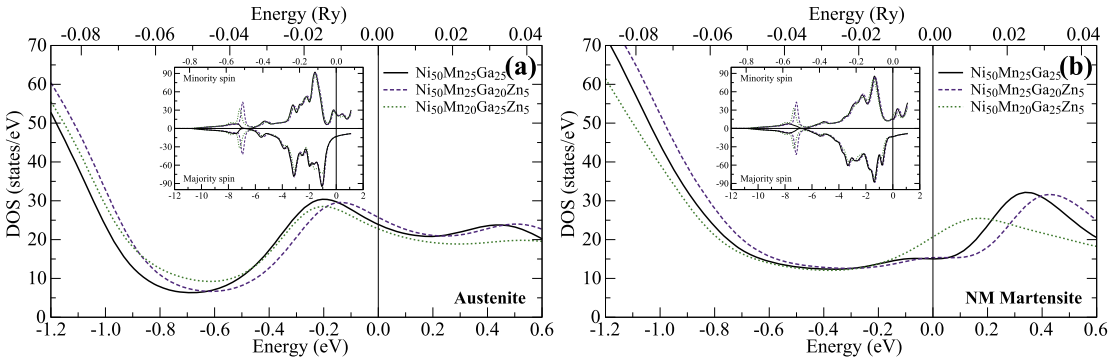

Figure 3. DOS in minority spin channel around the Fermi level, E_f, of cubic austenite (a) and NM martensite (b). Insets show DOS for both spin channels in broader range of energies. The zero on the x axis corresponds to E_f.

Table 2. Values of magnetic anisotropy energy MAE, magnetic moment μ_{tot}^{NM} and equilibrium c/a of NM martensite for alloys with different compositions calculated with help of PAW method.

Alloy	MAE (meV/atom)	μ_{tot}^{NM} (μ_B/f.u.)	c/a
$Ni_{50}Mn_{25}Ga_{25}$	−0.074	4.14	1.247
$Ni_{50}Mn_{25}(Ga_{18.75}Zn_{6.25})$	−0.054	4.06	1.257
$Ni_{50}(Mn_{18.75}Zn_{6.25})Ga_{25}$	−0.032	3.24	1.174
$Ni_{50}Mn_{25}(Ga_{18.75}Cu_{6.25})$	−0.028	4.10	1.257
$Ni_{50}(Mn_{18.75}Cu_{6.25})Ga_{25}$	−0.037	3.26	1.210

redistribution of electrons with resulting reduction of total energy [64–66]. The size and position of the antibonding peak is responsible for the instability of austenite, since high DOS near E_f increases the total energy of the cubic phase. The tetragonal distortion is accompanied with shifting of the antibonding peak trough E_f. The energy of the system first increases until the top of the peak reaches the Fermi level which creates an energy barrier in the tetragonal deformation path. Further tetragonal deformation results in further shifting of the peak and subsequently in decreasing of DOS at E_f as well as decreasing of total energy in martensite [33].

The total DOS of austenite phase for stoichiometric Ni_2MnGa and doped alloys is compared in figure 3(a). In austenite, the substitution of Ga by Zn moves both the pseudogap and the antibonding peak closer to E_f and increases DOS at E_f compared to the stoichiometric alloy. These effects are responsible for destabilization of the cubic austenite. On the contrary, substitution of Mn atoms by Zn fills the pseudogap and lowers the antibonding peak. This behavior is linked to the stabilization of austenite and consequently to the decrease in T_M.

The stability of martensitic phase in the stoichiometric alloy is enhanced by the shift of the antibonding peak above the Fermi level as shown in figure 3(b). Similarly, the doping on Ga sublattice results in a shift of both pseudogap and antibonding peak towards higher energies. The pseudogap in DOS of the stoichiometric alloy is slightly deeper and the minimization of DOS of Ga deficient alloy on the Fermi level is not present. Hence an increase in T_M is caused by destabilization of the austenitic phase.

On the other hand, doping on Mn sublattice affects neither pseudogap position nor its depth. A shift of the antibonding peak over E_f is not as strong as for the Ga substitution and not even as in the Ni_2MnGa alloy, hence stability of martensite is less resounding (figure 3(b)).

3.5. Magnetic anisotropy energy

Magnetic anisotropy energies (MAE) for different alloy compositions with 6.25 at. % of doping element calculated using PAW method are summarized in table 2 together with magnetic moment and c/a of NM martensite. We calculated also Cu doping for the sake of comparison. Equilibrium c/a of doped alloys calculated by PAW method agree well with those provided by EMTO-CPA method (see table 1 for Zn-doping and figure 4 in [33] for Cu-doping). The only difference is that PAW method predicts small increase of c/a for Zn-doping on the Ga-sublattice (Zn → Ga), whereas EMTO-CPA predicts small decrease. However, the deviation from c/a of stoichiometric alloy is very small in both methods and this difference can be neglected. All studied compositions exhibit negative MAE, which indicates preferred magnetisation in (001) plane. MAE of NM martensite with

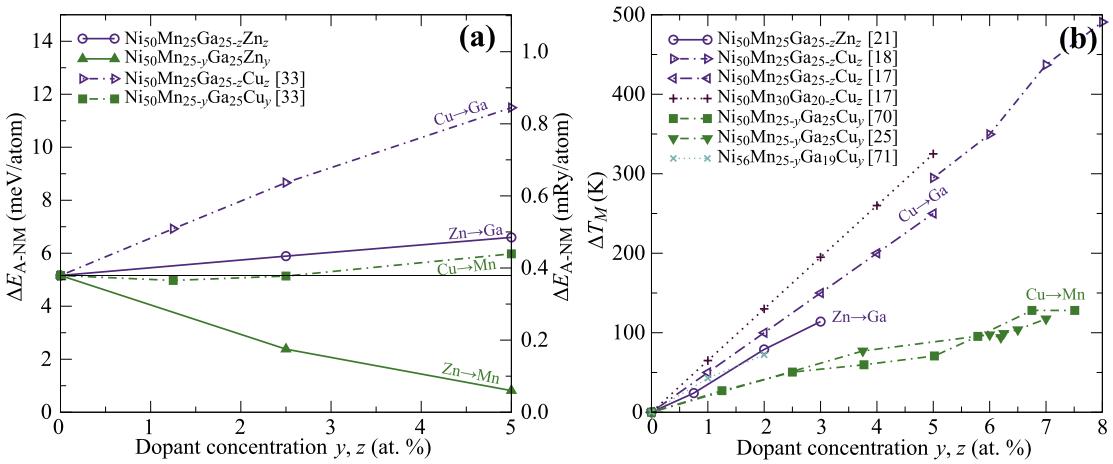

Figure 4. (a) Energy differences between austenite and NM martensite $\Delta E_{\mathrm{A-NM}}$ in FM state for different doping concentration of Zn compared to Cu-doped alloys. The thin horizontal line corresponds to $\Delta E_{\mathrm{A-NM}}$ of stoichiometric Ni_2MnGa. (b) Experimentally measured differences in martensitic transformation temperature ΔT_M as a function of dopant concentration y and z for different types of doping.

stoichiometric composition is equal to −0.074 meV/atom which is in good agreement with other calculated values −0.08 meV/atom reported in previous works [67–69].

Both Zn-doping and Cu-doping have a similar effect on magnetic moments and they decrease the anisotropy. However, the anisotropy decrease depends strongly on doping element and doped sublattice. The Zn-doping on the Ga sublattice results in about 30% decrease of MAE in comparison to the stoichiometric alloy but the MAE is still nearly twice larger than for the case of Cu doping on the Ga sublattice. On the other hand the Zn- and Cu-doping on Mn sublattice results in about 50% drop in MAE in comparison to stoichiometric alloy, with the Cu doping exhibiting MAE slightly larger than Zn doping. Such behaviour indicates, that Cu is responsible for significant decrease of magnetic anisotropy in Co- and Cu-doped alloy [20]. Thus, the replacement of Cu by Zn could result in higher magnetic anisotropy of the modified alloy.

The different effect of Cu and Zn doping on MAE originates in different localization of Cu and Zn atomic orbital in Ni-Mn-Ga alloy. Whereas the Cu d states exhibit wide bands lying approximately from −5 to −1 eV bellow Fermi level (see [33] and [62]), the Zn d and s states are strongly localized in very narrow band at −7 eV bellow Fermi level (see Supplementary material stacks.iop.org/MRX/7/026101/mmedia). Thus the states near the Fermi level responsible for MAE are more affected by the presence of Cu than the presence of Zn in the alloy.

4. Discussion

To predict the behavior of T_M in doped alloys the energy differences $\Delta E_{\mathrm{A-NM}}$ are plotted in figure 4(a) as a function of concentration of doping elements. The onset of plotted lines at concentration equal to zero represents the austenite-martensite total energy difference for stoichiometric Ni_2MnGa. The assumption is that all the ascending lines represent alloys with higher T_M compared to the unmodified alloy. In particular, the line representing Zn-doping on the Ga-sublattice (Zn → Ga) indicate that this doping should increase T_M whereas doping on Mn-sublattice (Zn → Mn) is expected to decrease T_M. Results computed in this work are compared with Cu-doping [33]. For Cu-doping on both Ga and Mn sublattices (Cu → Ga and Cu → Mn) $\Delta E_{\mathrm{A-NM}}$ dependencies ascend, predicting the increase in T_M. Theoretical predictions may be compared with available experimental results summarized in figure 4(b).

In all cases, theoretically obtained ascending lines correlate with experimentally observed increase in T_M. Moreover, the steepness of theoretical lines predicts the rate of growth of T_M as follows from the comparison of theoretical and experimental results. It predicts the weaker effect for Zn-doping than Cu-doping on Ga sublattice but stronger than Cu-doping on Mn sublattice [25, 70]. As can be also seen from figure 4(b), the effect of doping can be further enhanced when used in combination with off-stoichiometric Ni-Mn-Ga composition [17, 71].

Predictions of T_C are based on the study of energy differences between FM and PM states, $\Delta E_{\mathrm{PM-FM}}$. Since all structures were calculted at 0 K, we cannot say whether martensitic transformation takes place at lower temperature than magnetic transformation or if the Curie temperature of martensite T_C^M equals T_C^A of austenite. Hence, we focus on both $T_C^M \sim \Delta E^M_{\mathrm{PM-FM}}$ and $T_C^A \sim \Delta E^A_{\mathrm{PM-FM}}$. Again, it is supposed that the increase of $\Delta E_{\mathrm{PM-FM}}$ corresponds to a rise in T_C.

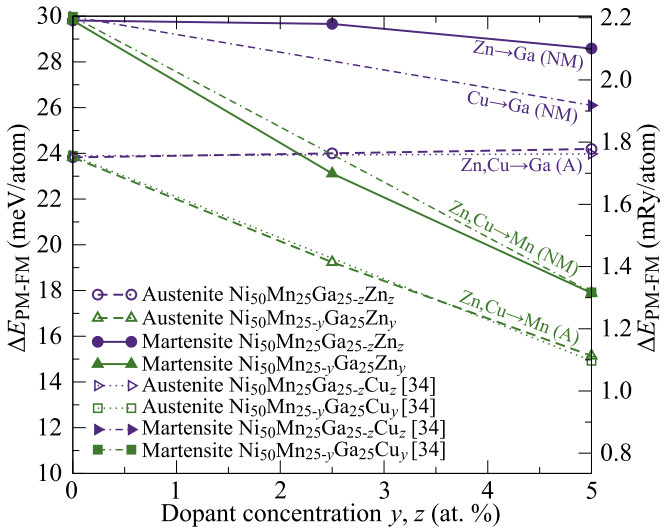

Figure 5. Comparison of energy differences between PM and FM states, $\Delta E_{\mathrm{PM-FM}}$, of Zn and Cu-doped alloys in austenite and NM martensite.

Results presented in figure 5 compare effects of doping with Zn and Cu on $\Delta E_{\mathrm{PM-FM}}$. It is shown that for doping on Mn-sublattice, the energy difference of FM and PM austenite, $\Delta E^{A}_{\mathrm{PM-FM}}$, is smaller for Zn-doped alloys than for the unmodified alloy, which can be related to reduction of magnetic moments (see table 1) in modified alloys. The same decrease of $\Delta E_{\mathrm{PM-FM}}$ can be seen also for tetragonal phase. This predicts the decrease in Curie temperature in both phases. Since NM martensite in PM state is unstable with respect to tetragonal deformation for doping with Zn as can be seen in figure 2(b), we used the total energy corresponding to the structure of stoichiometric NM martensite in FM state with $c/a = 1.14$ for estimation of $\Delta E_{\mathrm{PM-FM}}$. Using this approach we see that the substitution of Mn atoms by Zn results in lowering of both T_M and T_C at studied concentrations. Doping with Cu on Mn-sublattice has very similar effect on $\Delta E_{\mathrm{PM-FM}}$ as Zn-doping for both austenite and martensite, therefore Zn and Cu affect ΔT_C equally.

Considering the substitution of Ga atoms, figure 5 shows weakly descending dependences for transformation in martensite when doped with Zn atoms. Doping with Cu at Ga sites results in steeper decrease of $\Delta E^{M}_{\mathrm{PM-FM}}$, which predicts stronger decrease in Curie temperature compared to Zn-doped alloys. In austenite the dependences are almost constant and values of $\Delta E^{A}_{\mathrm{PM-FM}}$ are very close to each other for both types of doping.

Our results show that doping of Ni-Mn-Ga alloys by Zn exhibits effects comparable to Cu doping. Simultaneous doping with Zn and an element increasing T_C (Co [72] or Fe [73, 74] on Ni sublattice) may result in similar enhancement of properties as in the case of Ni-Mn-Ga-Cu-Co alloy, with significant increase in both T_M and T_C [15], where Co compensates negative effect of Cu on T_C. Further improvement of MFIS can be expected if we consider also significantly higher magnetic anisotropy predicted for Zn-doped alloy. Zn-doping on Ga sublattice decreases the MAE much less than Cu-doping.

The calculated behavior can be compared with the $T_M \sim e/a$ phenomenological rule. If we assume Zn having 12 valence electrons, which is more than number of valence electrons in Ga or Mn, doping by Zn on both sublattices should should raise T_M. This prediction is qualitatively correct for substitution of Ga atoms. As Zn has more valence electron than Cu, the effect of Zn should be even stronger and T_M should grow more steeply than in Cu-doped alloys. This, however, does not agree with our theoretical prediction based on $\Delta E_{\mathrm{A-NM}}$ and experimental results (figure 4). Moreover, the e/a rule fails completely for doping on Mn sublattice, where T_M drops with growing concentration of Zn. On the other hand, if we consider that Zn has only 2 valence s-electrons, the decrease in T_M is expected for doping on both Mn and Ga sublattice, which is also not seen. Apparently the simple rule of valence electron concentration is not applicable to Zn-doped alloys and alternative methods such as *ab initio* calculations are needed.

5. Conclusions

The development of martensitic transformation temperature, T_M, and Curie temperature, T_C, in Zn-doped Ni-Mn-Ga magnetic shape memory alloys was predicted with the help of first-principles calculation employing EMTO-CPA method. The prediction of trends in T_M as a function of concentration of doping element is based

upon calculated energy differences between the cubic structure of austenite and the tetragonal structure of NM martensite, ΔE_{A-NM}, whereas the energy difference between paramagnetic and ferromagnetic states ΔE_{PM-FM} serves for estimation of trends in T_C. Although used calculations can be considered rudimentary the calculated trends for T_M and T_C provide important guide for experimentalist and theorist alike. For more quantitative calculation of T_M, more detailed method based on lattice dynamics should be used. The same is valid for T_C where the mean field approximation or Monte Carlo method can be used.

The alloys with Zn substituted on Ga-sublattice exhibit stabilization of NM martensite compared to austenite, which results in the increase in T_M. In contrast, if Mn-sublattice is occupied by Zn then NM martensite is destabilized and its equilibrium $(c/a)_{NM}$ decreases and the decrease in T_M can be expected. This finding is not in agreement with the empirical rule found e.g. for Cu-doping that T_M should increase with increasing concentration of valence electron per atom, e/a, and it casts doubt upon general validity of the $T_M \sim e/a$ rule for Ni-Mn-Ga system, as indicated also before [21].

Substitution of Ga by Zn does not have significant effect on ΔE_{PM-FM} in austenite hence a very small effect on T_C can be expected. In martensite, ΔE_{PM-FM} decreases only slightly. Calculated ΔE_{PM-FM} in NM martensite is smaller than for Cu-doped alloys, thus Zn on Ga sublattice decreases T_C less significantly than Cu on the same sublattice. A much stronger decrease of ΔE_{PM-FM} in both phases was observed when Zn was substituted for Mn, which suggests stronger decrease in T_C.

Moreover, a beneficial effect of Zn can be expected for magnetic anisotropy of NM martensite. Whereas Cu on Ga sublattice significantly decreases MAE, the decrease is only moderate in case of Zn doping on Ga sublattice. Zn thus seems to be a suitable candidate to replace Cu in Ni-Mn-Ga-Co-Cu alloys.

Acknowledgments

The work of J Janovec, M Zelený L Straka, and O Heczko was supported by the Ministry of Education, Youth and Sports of the Czech Republic within the program OP VVV 'Excellent Research Teams' under Project CZ.02.1.01/0.0/0.0/15_003/0000487-MATFUN, within the support program 'National Sustainability Programme I' under Project NETME CENTRE PLUS LO1202, by the Large Infrastructures for Research, Experimental Development and Innovations projects 'CERIT Scientific Cloud LM2015085' and 'IT4Innovations National Supercomputing Center-LM2015070', and by the Czech Science Foundation under project no. 16-00043S. The work of A. Sozinov was supported by the Strategic Research Council (SRC) of Finland through the grant no. 313349.

ORCID iDs

Martin Zelený https://orcid.org/0000-0001-6715-4088

References

[1] Likhachev A A and Ullakko K 2000 Quantitative model of large magnetostrain effect in ferromagnetic shapell memory alloys *Eur. Phys. J.* B **14** 263–7
[2] Heczko O 2005 Magnetic shape memory effect and magnetization reversal *J. Magn. Magn. Mater.* **290–291** 787–94
[3] Murray S J, Marioni M, Allen S M, O'Handley R C and Lograsso T A 2000 6% magnetic-field-induced strain by twin-boundary motion in ferromagnetic Ni–Mn–Ga *Appl. Phys. Lett.* **77** 886–8
[4] Heczko O, Sozinov A and Ullakko K 2000 Giant field-induced reversible strain in magnetic shape memory NiMnGa alloy *IEEE Trans. Mag.* **36** 3266–8
[5] Sozinov A, Likhachev A A, Lanska N and Ullakko K 2002 Giant magnetic-field-induced strain in NiMnGa seven-layered martensitic phase *Appl. Phys. Lett.* **80** 1746–8
[6] Okamoto N, Fukuda T and Kakeshita T 2008 Temperature dependence of rearrangement of martensite variants by magnetic field in 10M, 14M and 2M martensites of Ni-Mn-Ga alloys *Mater. Sci. Eng.* A **481–482** 306–9
[7] Heczko O, Straka L, Novak V and Fähler S 2010 Magnetic anisotropy of nonmodulated Ni-Mn-Ga martensite revisited *J. Appl. Phys.* **107** 09A914
[8] Zelený M, Straka L, Sozinov A and Heczko O 2016 Ab initio prediction of stable nanotwin double layers and 4O structure in Ni_2MnGa *Phys. Rev.* B **94** 224108
[9] Webster P J, Ziebeck K R A, Town S L and Peak M S 1984 Magnetic order and phase transformation in Ni_2MnGa *Philos. Mag.* B **49** 295–310
[10] Schlüter K, Holtz B and Raatz A 2012 Principle design of actuators driven by magnetic shape memory alloys *Adv. Eng. Mater.* **14** 682–6
[11] Karaman I, Basaran B, Karaca H E, Karsilayan A I and Chumlyakov Y I 2007 Energy harvesting using martensite variant reorientation mechanism in a NiMnGa magnetic shape memory alloy *Appl. Phys. Lett.* **90** 172505
[12] Rolfs K, Chmielus M, Wimpory R, Mecklenburg A, Müllner P and Schneider R 2010 Double twinning in Ni–Mn–Ga–Co *Acta Mater.* **58** 2646–51
[13] Pérez-Checa A, Feuchtwanger J, Barandiaran J, Sozinov A, Ullakko K and Chernenko V 2018 Ni-Mn-Ga-(Co, Fe, Cu) high temperature ferromagnetic shape memory alloys: Effect of Mn and Ga replacement by Cu *Scr. Mater.* **154** 131–3

[14] Pérez-Checa A, Musiienko D, Saren A, Soroka A, Feuchtwanger J, Sozinov A, Barandiaran J, Ullakko K and Chernenko V 2019 Study of the critical parameters for magnetic field-induced strain in high temperature Ni-Mn-Ga-Co-Cu-Fe single crystals *Scr. Mater.* **158** 16–9

[15] Sozinov A, Lanska N, Soroka A and Zou W 2013 12% magnetic field-induced strain in Ni-Mn-Ga-based non-modulated martensite *Appl. Phys. Lett.* **102** 021902

[16] Glavatskyy I, Glavatska N, Dobrinsky A, Hoffmann J-U, Söderberg O and Hannula S-P 2007 Crystal structure and high-temperature magnetoplasticity in the new Ni–Mn–Ga–Cu magnetic shape memory alloys *Scr. Mater.* **56** 565–8

[17] Jiang C, Wang J, Li P, Jia A and Xu H 2009 Search for transformation from paramagnetic martensite to ferromagnetic austenite: NiMnGaCu alloys *Appl. Phys. Lett.* **95** 012501

[18] Li Y, Wang J and Jiang C 2011 Study of Ni-Mn-Ga-Cu as single-phase wide-hysteresis shape memory alloys *Mater. Sci. Eng.* A **528** 6907–11

[19] Soto-Parra D E, Moya X, Mañosa L, Planes A, Flores-Zúñiga H, Alvarado-Hernández F, Ochoa-Gamboa R A, Matutes-Aquino J A and Ríos-Jara D 2010 Fe and Co selective substitution in Ni2MnGa: Effect of magnetism on relative phase stability *Philos. Mag.* **90** 2771–92

[20] Rameš M, Heczko O, Sozinov A, Ullakko K and Straka L 2018 Magnetic properties of Ni-Mn-Ga-Co-Cu tetragonal martensites exhibiting magnetic shape memory effect *Scr. Mater.* **142** 61–5

[21] Barton L S, Lazott R T and Marsten E R 2014 Magnetic properties of full Heusler alloys $Ni_2MnGa_{1-x}Z_x$ with Z=Sn or Zn *J. Appl. Phys.* **115** 17A908

[22] Chernenko V 1999 Compositional instability of β-phase in Ni-Mn-Ga alloys *Scr. Mater.* **40** 523–7

[23] Lanska N, Söderberg O, Sozinov A, Ge Y, Ullakko K and Lindroos V K 2004 Composition and temperature dependence of the crystal structure of Ni–Mn–Ga alloys *J. Appl. Phys.* **95** 8074–8

[24] Chakrabarti A, Siewert M, Roy T, Mondal K, Banerjee A, Gruner M E and Entel P 2013 Ab initio studies of effect of copper substitution on the electronic and magnetic properties of Ni_2 MnGa and Mn_2NiGa *Phys. Rev.* B **88** 174116

[25] Sarkar S K, Sarita, Babu P D, Biswas A, Siruguri V and Krishnan M 2016 Giant magnetocaloric effect from reverse martensitic transformation in Ni–Mn–Ga–Cu ferromagnetic shape memory alloys *J. Alloys Compd.* **670** 281–8

[26] Greenwood N N and Earnshaw A 2012 *Chemistry of the Elements* 2nd edn (Butterworth Heinemann, Oxford: Elsevier Science & Technology)

[27] Jiang C, Muhammad Y, Deng L, Wu W and Xu H 2004 Composition dependence on the martensitic structures of the Mn-rich NiMnGa alloys *Acta Mater.* **52** 2779–85

[28] Chen J, Li Y, Shang J and Xu H 2006 First principles calculations on martensitic transformation and phase instability of Ni–Mn–Ga high temperature shape memory alloys *Appl. Phys. Lett.* **89** 231921

[29] Barman S R, Chakrabarti A, Singh S, Banik S, Bhardwaj S, Paulose P L, Chalke B A, Panda A K, Mitra A and Awasthi A M 2008 Theoretical prediction and experimental study of a ferromagnetic shape memory alloy: Ga_2MnNi *Phys. Rev.* B **78** 134406

[30] Staunton J B 1994 The electronic structure of magnetic transition metallic materials *Rep. Prog. Phys.* **57** 1289

[31] Sato K, Katayama-Yoshida H and Dederichs P H 2005 Dilute magnetic semiconductors *Psi-K Newsletter* **70** 93–110 (https://psi-k.net/download/highlights/Highlight_70.pdf)

[32] Dutta B, Bhandary S, Ghosh S and Sanyal B 2012 First-principles study of magnetism in Pd_3Fe under pressure *Phys. Rev.* B **86** 024419

[33] Zelený M, Sozinov A, Straka L, Björkman T and Nieminen R M 2014 First-principles study of Co- and Cu-doped Ni_2MnGa along the tetragonal deformation path *Phys. Rev.* B **89** 184103

[34] Zelený M, Sozinov A, Björkman T, Straka L, Heczko O and Nieminen R M 2017 Effect of magnetic ordering on the stability of Ni–Mn–Ga(–Co–Cu) alloys along the tetragonal deformation path *IEEE Trans. Magn.* **53** 1700306

[35] Hickel T, Uijttewaal M, Al-Zubi A, Dutta B, Grabowski B and Neugebauer J 2012 Ab initio-based prediction of phase diagrams: application to magnetic shape memory alloys *Adv. Eng. Mater.* **14** 547–61

[36] Entel P, Dannenberg A, Siewert M, Herper H C, Gruner M E, Buchelnikov V D and Chernenko V A 2011 Composition-dependent basics of smart heusler materials from first-principles calculations *Mat. Sci. Forum* **684** 1–29

[37] Andersen O K, Jepsen O and Krier G 1995 Exact Muffin-Tin Orbital Theory *Lectures on Methods of Electronic Structure Calculations* ed V Kumar, O K Andersen and A Mookerjee (Singapore: World Scientific) pp 63–124

[38] Vitos L 2007 *Computational Quantum Mechanics for Materials Engineers* (London: Springer) (https://doi.org/10.1007/978-1-84628-951-4)

[39] Szunyogh L, Újfalussy B, Weinberger P and Kollár J 1994 Self-consistent localized KKR scheme for surfaces and interfaces *Phys. Rev.* B **49** 2721–9

[40] Vitos L 2001 Total-energy method based on the exact muffin-tin orbitals theory *Phys. Rev.* B **64** 014107

[41] Perdew J P, Burke K and Ernzerhof M 1996 Generalized gradient approximation made simple *Phys. Rev. Lett.* **77** 3865–8

[42] Li C-M, Hu Q-M, Yang R, Johansson B and Vitos L 2011 Interplay between temperature and composition effects on the martensitic transformation in $Ni_{2+x}Mn_{1-x}Ga$ alloys *Appl. Phys. Lett.* **98** 261903

[43] Hu Q-M, Luo H-B, Li C-M, Vitos L and Yang R 2012 Composition dependent elastic modulus and phase stability of Ni_2MnGa based ferromagnetic shape memory alloys *Sci. China Tech. Sci.* **55** 295

[44] Gyorffy B L, Pindor A J, Staunton J, Stocks G M and Winter H 1985 A first-principles theory of ferromagnetic phase transitions in metals *J. Phys. F: Met. Phys.* **15** 1337

[45] Soven P 1967 Coherent-potential model of substitutional disordered alloys *Phys. Rev.* **156** 809–13

[46] Vitos L, Abrikosov I A and Johansson B 2001 Anisotropic lattice distortions in random alloys from first-principles theory *Phys. Rev. Lett.* **87** 156401

[47] Korzhavyi P A, Ruban A V, Abrikosov I A and Skriver H L 1995 Madelung energy for random metallic alloys in the coherent potential approximation *Phys. Rev.* B **51** 5773–80

[48] Ruban A V and Skriver H L 2002 Screened Coulomb interactions in metallic alloys. I. universal screening in the atomic-sphere approximation *Phys. Rev.* B **66** 024201

[49] Daalderop G H O, Kelly P J and Schuurmans M F H 1990 First-principles calculation of the magnetocrystalline anisotropy energy of iron, cobalt, and nickel *Phys. Rev.* B **41** 11919–37

[50] Kresse G and Furthmüller J 1996 Efficient iterative schemes for *ab initio* total-energy calculations using a plane-wave basis set *Phys. Rev.* B **54** 11169–86

[51] Kresse G and Furthmüller J 1996 Efficiency of ab-initio total energy calculations for metals and semiconductors using a plane-wave basis set *Comput. Mater. Sci.* **6** 15–50

[52] Blöchl P E 1994 Projector augmented-wave method *Phys. Rev.* B **50** 17953–79

[53] Kresse G and Joubert D 1999 From ultrasoft pseudopotentials to the projector augmented-wave method *Phys. Rev.* B **59** 1758–75

[54] Methfessel M and Paxton A T 1989 High-precision sampling for Brillouin-zone integration in metals *Phys. Rev.* B **40** 3616–21

[55] Luo H-B, Hu Q-M, Li C-M, Yang R, Johansson B and Vitos L 2012 Phase stability of $Ni_2(Mn_{1-x}Fe_x)Ga$: A first-principles study *Phys. Rev.* B **86** 024427
[56] Yin M, Nash P, Chen W and Chen S 2016 Standard enthalpies of formation of selected Ni2YZ heusler compounds *J. Alloys Compd.* **660** 258–65
[57] Ni Z, Guo X, Li Q, Liang Z, Luo H and Meng F 2018 Effect of Zn-doping on the phase transition and magnetic properties of Heusler alloys $Ni_2MnGa_{1-x}Zn_x$ ($x = 0, 0.25, 0.5, 0.75$ and 1) *J. Magn. Magn. Mater.* **464** 65–70
[58] Enkovaara J, Heczko O, Ayuela A and Nieminen R M 2003 Coexistence of ferromagnetic and antiferromagnetic order in Mn-doped Ni_2MnGa *Phys. Rev.* B **67** 212405
[59] Ayuela A, Enkovaara J and Nieminen R M 2002 Ab initio study of tetragonal variants in Ni_2MnGa alloy *J. Phys. Condens. Matter* **14** 5325
[60] Zayak A T, Entel P, Enkovaara J, Ayuela A and Nieminen R M 2003 First-principles investigations of homogeneous lattice-distortive strain and shuffles in Ni_2MnGa *J. Phys. Condens. Matter* **15** 159
[61] Ghosh S, Vitos L and Sanyal B 2011 Structural and elastic properties of $Ni_{2+x}Mn_{1-x}Ga$ alloys *Physica* B **406** 2240–4
[62] Li C-M, Luo H-B, Hu Q-M, Yang R, Johansson B and Vitos L 2011 Site preference and elastic properties of Fe-, Co-, and Cu-doped Ni_2MnGa shape memory alloys from first principles *Phys. Rev.* B **84** 024206
[63] Li C-M, Luo H-B, Hu Q-M, Yang R, Johansson B and Vitos L 2010 First-principles investigation of the composition dependent properties of $Ni_{2+x}Mn_{1-x}Ga$ shape-memory alloys *Phys. Rev.* B **82** 024201
[64] Fujii S, Ishida S and Asano S 1989 Electronic structure and lattice transformation in Ni_2MnGa and Co_2NbSn *J. Phys. Soc. Jpn.* **58** 3657–65
[65] Brown P J, Bargawi A Y, Crangle J, Neumann K-U and Ziebeck K R A 1999 Direct observation of a band Jahn-Teller effect in the martensitic phase transition of Ni_2MnGa *J. Phys. Condens. Matter* **11** 4715
[66] Özdemir Kart S, Uludoğan M, Karaman I and Çağın T 2008 DFT studies on structure, mechanics and phase behavior of magnetic shape memory alloys: Ni_2MnGa *Phys. Stat. Solidi (a)* **205** 1026–35
[67] He W Q, Ma X Q, Liu Z H, Wang Y and Chen L-Q 2017 Magnetic anisotropy energy of ferromagnetic shape memory alloys Ni_2X(X = Fe,Co)Ga by first-principles calculations *AIP Adv.* **7** 075001
[68] Caron L *et al* 2017 Effect of Pt substitution on the magnetocrystalline anisotropy of Ni_2MnGa: a competition between chemistry and elasticity *Phys. Rev.* B **96** 054105
[69] Herper H C 2018 Ni-based Heusler compounds: how to tune the magnetocrystalline anisotropy *Phys. Rev.* B **98** 014411
[70] Kataoka M, Endo K, Kudo N, Kanomata T, Nishihara H, Shishido T, Umetsu R Y, Nagasako M and Kainuma R 2010 Martensitic transition, ferromagnetic transition, and their interplay in the shape memory alloys $Ni_2Mn_{1-x}Cu_xGa$ *Phys. Rev.* B **82** 214423
[71] Ma Y, Yang S, Jin W and Liu X 2009 $Ni_{56}Mn_{25-x}Cu_xGa_{19}$ ($x = 0, 1, 2, 4, 8$) high-temperature shape-memory alloys *J. Alloys Compd.* **471** 570–4
[72] Cong D Y, Wang S, Wang Y D, Ren Y, Zuo L and Esling C 2008 Martensitic and magnetic transformation in Ni-Mn-Ga-Co ferromagnetic shape memory alloys *Mater. Sci. Eng.* A **473** 213–8
[73] Soto D, Hernández F A, Flores-Zúñiga H, Moya X, Mañosa L, Planes A, Aksoy S, Acet M and Krenke T 2008 Phase diagram of Fe-doped Ni-Mn-Ga ferromagnetic shape-memory alloys *Phys. Rev.* B **77** 184103
[74] Khovailo V V, Abe T, Koledov V V, Matsumoto M, Nakamura H, Note R, Ohtsuka M, Shavrov V G and Takagi T 2003 Influence of Fe and Co on phase transitions in Ni-Mn-Ga alloys *Mater. Trans.* **44** 2509–12